THE JOURNAL OF PHYSICAL CHEMISTRY C

Article

pubs.acs.org/JPCC

Plasmonic Interactions at Close Proximity in Chiral Geometries: Route toward Broadband Chiroptical Response and Giant Enantiomeric Sensitivity

Greshma Nair,[†,⊥] Haobijam Johnson Singh,[‡,⊥] Debadrita Paria,[†] Murugesan Venkatapathi,[§] and Ambarish Ghosh*[,†,‡,∥]

[†]Centre for Nano Science and Engineering, Indian Institute of Science, Bangalore 560012, India

[‡]Department of Physics, Indian Institute of Science, Bangalore 560012, India

[§]Computational Photonics Laboratory, SERC, Indian Institute of Science, Bangalore 560012, India

[∥]Department of Electrical Communications Engineering, Indian Institute of Science, Bangalore 560012, India

Supporting Information

ABSTRACT: Chiral metamaterials can have diverse technological applications, such as engineering strongly twisted local electromagnetic fields for sensitive detection of chiral molecules, negative indices of refraction, broadband circular polarization devices, and many more. These are commonly achieved by arranging a group of noble-metal nanoparticles in a chiral geometry, which, for example, can be a helix, whose chiroptical response originates in the dynamic electromagnetic interactions between the localized plasmon modes of the individual nanoparticles. A key question relevant to the chiroptical response of such materials is the role of plasmon interactions as the constituent particles are brought closer, which is investigated in this paper through theoretical and experimental studies. The results of our theoretical analysis, when the particles are brought in close proximity are dramatic, showing a large red shift and enhancement of the spectral width and a near-exponential rise in the strength of the chiroptical response. These predictions were further confirmed with experimental studies of gold and silver nanoparticles arranged on a helical template, where the role of particle separation could be investigated in a systematic manner. The "optical chirality" of the electromagnetic fields in the vicinity of the nanoparticles was estimated to be orders of magnitude larger than what could be achieved in all other nanoplasmonic geometries considered so far, implying the suitability of the experimental system for sensitive detection of chiral molecules.

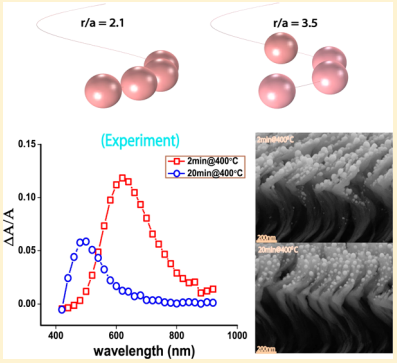

INTRODUCTION

Strong light matter interactions in metallic nanoparticles (NPs), especially those made of noble metals such as gold and silver, is at the heart of much ongoing research in nanophotonics. Individual NPs can support collective excitations (plasmons) of the electron plasma at certain wavelengths, known as the localized surface plasmon resonance (LSPR),[1] which forms the basis of bright colors in colloidal solutions of Au and Ag and provides a powerful platform for various sensing, imaging, and therapeutic technologies.[2,3] It is interesting to note that the optical properties of a collection of NPs can be significantly different from isolated particles, an effect that originates in the electromagnetic interactions between the localized plasmon modes. This problem has been considered in one and two dimensions with periodic,[4−7] as well as with random,[8−10] arrays of NPs, and it was found that as the particles are brought closer, the plasmon resonances show distinct broadening, along with significant red or blue shifts in their spectral positions, where the sign of the shift depends on the direction of polarization with respect to the interparticle axes. With recent advances in nanotechnology, it has now been possible to develop wafer scale methods of fabricating 3-D arrays of NPs,[11,12] whose sizes and spacing could be engineered with high precision. Of great current interest is that of a chiral arrangement of NPs[13−16] that has been shown to give rise to strong chiroptical response in the visible, which for relatively small sizes of NPs (so that scattering can be neglected) is manifested in the differential absorption of circularly polarized light. These (chiral) metamaterials[17,18] can have properties with diverse technological applications, such as negative indices of refraction,[19,20] broadband circular polarization devices,[21,22] and so on, and may be used to engineer strongly twisted local electromagnetic fields in the vicinity of the NPs, which may aid in sensitive detection of chiral molecules.[23] The circular differential optical response of such materials originates in the dynamic Coulomb interaction between the NPs arranged in a 3-D chiral geometry and can be directly related to the retardation of the incident wave across the NP complex.[24,25] The standard semianalytical

Received: November 30, 2013
Revised: February 11, 2014
Published: February 11, 2014

 © 2014 American Chemical Society dx.doi.org/10.1021/jp4117535 | J. Phys. Chem. C 2014, 118, 4991−4997

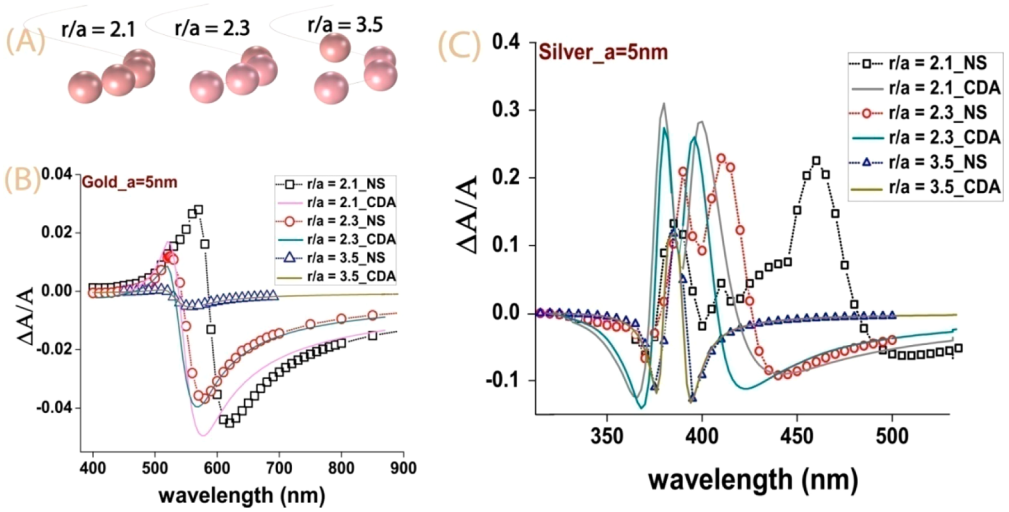

Figure 1. (A) Schematic of NPs arranged along a helix with different separations, corresponding to r/a = 2.1, 2.3, and 3.5. (B) Chiroptical asymmetry factor as a function of wavelength for r/a = 2.1, 2.3, and 3.5, as obtained from numerical simulations (NS). The NPs were assumed to be made of Au with radius 5 nm, and the surrounding medium was assumed to water (ε_m = 1.78). Also shown (solid lines) are the results of the semianalytical (CDA) calculations. (C) Same as panel B, except the NPs are assumed to be of Ag.

approach to calculate the chiroptical properties, for example, circular dichroism (CD) of such model systems, is applicable for particle separations somewhat larger than their dimensions, such that each NP can be approximated simply as an oscillating electric dipole moment, induced by the combined electric fields from the neighboring NPs and the incident electromagnetic field.

The aim of this study is to investigate the effect of interparticle separation on the chiroptical response, especially in the regime where it may be insufficient to consider the NP assembly as interacting dipoles ("coupled dipole approximation"), but instead it becomes necessary to consider higher order multipolar contributions to the electromagnetic coupling between various NPs. As obtained from theoretical[7,26−28] and experimental[29,30] studies with model 1 and 2-D NP arrays, the contributions from the higher order modes are non-negligible when the center to center distances (r) are less than three times the particle radius (a), that is, $r < 3a$, a regime that describes the NP interactions beyond the so-called couple dipole approximation. As shown in the study presented here, dipole approximation continues to be valid until around $r/a \approx 2.3$, below which the multipolar contributions play an important role. Most interestingly, the strength of the chiroptical response increases in a near-exponential fashion as the particles are brought in tighter confinement (even for $r/a > 3$), along with a significant shift and broadening of the CD spectrum. These predictions were confirmed with our experimental studies, where we measured the chiroptical spectra of various sizes and separations of NPs arranged in a helical geometry. The experimental system, as we show later, had a variability in the sizes and separations of the NPs, which resulted in a broader spectral response than predicted, an effect that could be used for fabricating chiral metamaterials with broadband response in the visible. Finally, tighter confinement of the NPs was found to increase the "chirality parameter" of the electromagnetic fields around the NP complex, with a degree of enhancement much larger than what has been predicted in any other chiroplasmonic system so far, an effect that can be exploited for developing a sensitive detection scheme for chiral molecules using "twisted" electromagnetic fields.[23,31]

RESULTS AND DISCUSSION

To investigate the role of interparticle separation on the chiroptical spectra, we considered a minimal model with four identical spherical NPs arranged on a helix, which is the minimum requirement to ensure the absence of any symmetry plane. The NPs were assumed to be of radius 5 nm, made of either gold (Au) or silver (Ag), arranged along a helix of pitch 25 nm and radius 18 nm (schematic shown in Figure 1A). The real and imaginary parts of the dielectric constants of Au and Ag were obtained from literature.[32] The dielectric permittivity (ε_m) of the medium surrounding the NPs was assumed to be wavelength-independent and corresponded to either air (ε_m = 1) or water (ε_m = 1.78). We calculated the optical absorption of the NP complex for left and right circularly polarized light, from where we estimated the asymmetry factor (g) in the chiroptical response, which was defined as the ratio of the differential (ΔA) to the average absorption (A) coefficients. Circular differential scattering has been neglected in this study, which is justified due to the low scattering contributions from NPs of such small sizes. The calculations were done with a numerical simulation (NS) using either discrete dipole approximation (DDSCAT)[33] or finite element calculation (COMSOL)[34,35] and semianalytically as well using the coupled dipole approximation (CDA).[36] The results obtained by DDSCAT were cross-checked with the finite element based numerical (COMSOL) simulation (comparison shown in the Supporting Information). The details of the numerical and semianalytical calculations have been provided in the methods and Supporting Information, respectively. The main variable in the model was chosen to be the interparticle distance r, obtained by altering the position of the NPs along the same helical geometry.

Typical chiroptical spectra for r/a = 3.5, 2.3, and 2.1 obtained from the numerical simulations along with the CDA-based calculations have been shown in Figure 1, where the asymmetry factor ($\Delta A/A$) of the NP complex is plotted as a function of wavelength. We assumed the particles (Au in Figure 1B, Ag in Figure 1C) to be embedded in water. The incident beam was assumed to be directed along the helix axis for all simulations and experiments presented here. The shape of the spectra remained qualitatively similar when r/a was changed from 3.5

dx.doi.org/10.1021/jp4117535 | J. Phys. Chem. C 2014, 118, 4991−4997

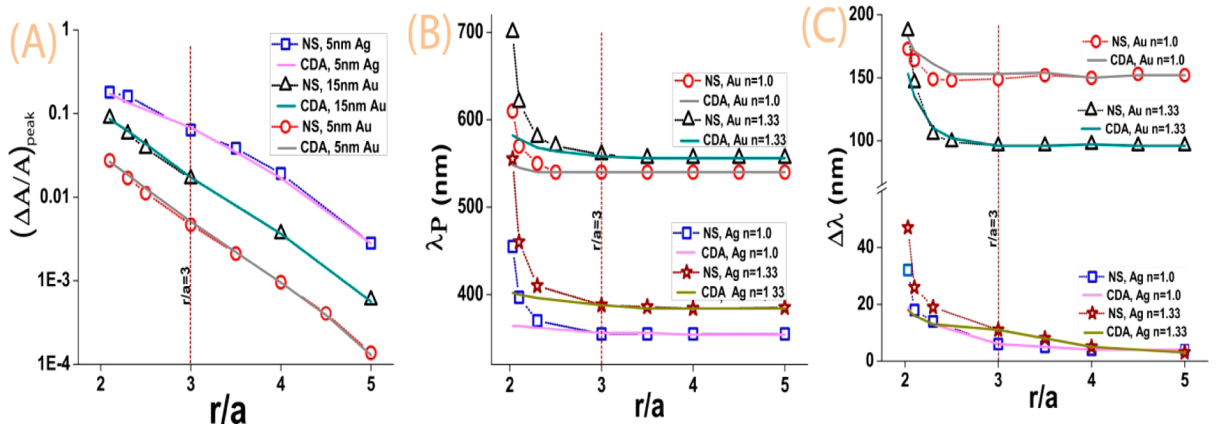

Figure 2. (A) Peak value (log scale) of the anisotropy factor as a function of r/a for Au (radius 5 and 15 nm) and Ag (5 nm), assumed to be in air. Similar trends were observed for different medium (e.g., water) surrounding the NPs, which has not been shown here for clarity. Both numerical (NS, symbols) and semianalytical (CDA, lines) calculations have been shown. (B) Wavelength corresponding to peak in the anisotropy factor, denoted by λ_p as a function of r/a for Ag and Au. The NPs were of radius 5 nm, embedded in either air or water. (C) fwhm spectral width ($\Delta\lambda$) as a function of r/a for Au and Ag. The NPs were of radius 5 nm, embedded in either air or water.

to 2.3, with a well-understood[24] dip-peak shape for Au and a double peak-single dip shape for Ag. Interestingly, however, the magnitude of the chiroptical signal increased manifold as the particles were brought closer (smaller r/a), with a significant red shift and increase in spectral width. The results of the numerical simulations and the semianalytical calculations were almost identical until about r/a = 2.3, below which there was a considerable difference between the two methods. Although there is no direct evidence, we believe this could be due to enhanced multipolar contributions to the chiroplasmonic interactions at very small separations.

To study the variation of the chiroptical spectra as a function of interparticle separation, we studied three parameters, corresponding to the maximum magnitude of $\Delta A/A$, the wavelength λ_p corresponding to the maximum of $\Delta A/A$, and the spectral width $\Delta\lambda$ corresponding to the full width at half-maximum of the spectra as a function of r/a. The results are shown in Figure 2. Typical CD spectra also showed similar behavior, and this has been included in the Supporting Information. The increase in the anisotropy factor $\Delta A/A$ was found to have a near-exponential dependence with r/a, as shown in Figure 2A, where the magnitude of the maximum value of the anisotropy factor, $(\Delta A/A)_{peak}$, is plotted as a function of r/a for Au and Ag NP complexes. It is interesting to note that the value of $(\Delta A/A)_{peak}$ serves as a strong indicator of the strength of the chiroptical signal, which increased when the NP sizes were increased (as shown for Au) and when Ag NPs were used. This is expected because larger dipole moments are induced in bigger NPs,[1] as observed for Au NPs of 5 and 15 nm radii, and stronger plasmonic effects are expected in Ag due to lower electromagnetic damping.[1] Correspondingly, λ_p and $\Delta\lambda$ also showed an increase (implying red shift and spectral broadening) as r/a was reduced below 3, which is qualitatively similar to the observations with absorption spectra of linear NP arrays when the polarization of the incident beam is parallel to the interparticle axis.[30] The rise in λ_p and $\Delta\lambda$ was found to be most dramatic below $r/a \approx 2.3$, where the results differed significantly from CDA predictions.

To confirm the predicted rise in $\Delta A/A$ as well as the predicted red shift and broadening of the chiroptical spectra for tighter NP separations experimentally, we have used a recently developed technique of fabricating chiral metamaterials, where metallic NPs were deposited at a grazing incidence to a dielectric (here, SiO_2) helical template.[37] Although initially nonspherical, the NPs can become spherical upon heating.[38,39] Upon continuation of the heating step, as shown in the SEM images shown in Figure 3A, the separation between the NPs can be controlled reasonably well, without significant variation in the particle size. Analyzing the SEM images of the nanostructured film (for Au) revealed that the average NP sizes increased from 7.5 to 9.5 nm upon heating, while the average r/a increased from 2.57 to 3.61. The corresponding asymmetry factors for these structures are shown in Figure 3B, where a clear increase in $\Delta A/A$ as well as spectral red shift and broadening could be clearly observed. The results for the Ag NP complex were found to be more dramatic, as shown in the spectra shown in Figure 3C. The average NP size remained constant for Ag to be 15 ± 3 nm, while r/a varied from 2.4 to 3.1 for different annealing times.

While the experimental results were in definite qualitative agreement with the theoretical predictions, the measured values of λ_p (~640 nm for Au and ~620 nm for Ag) and $\Delta\lambda$ (~115 nm for Au and ~185 nm for Ag) were observed to be significantly higher than what was expected (see Figure 1B,C) from the numerical calculations. In this context, it is important to point out the differences between the experimental system and the theoretical assumptions and to assess possible outcomes of these differences. For example, the numerical simulations as well as the semianalytical calculations were performed with four NPs, while the number of particles in the experimental system varied between 60 and 90. We argue this should not affect the general conclusions because the quantity of interest was chosen to be the ratio $\Delta A/A$, where both A and ΔA are expected to increase similarly as the number of NPs is increased. Another difference was due to the inherent structure of the nanostructured films, where the medium surrounding the NPs was partially air (ε_m = 1) and partially SiO_2 (ε_m = 1.5). However, as seen from the theoretical results shown in Figure 2B,C, the manner in which the peak wavelength and the spectral width varied with r/a was very similar, irrespective of the dielectric permittivity of the surrounding medium. We have performed a numerical simulation including the presence of the dielectric template and did not find a large role of the SiO2 template, when the surrounding medium was assumed to be

dx.doi.org/10.1021/jp4117535 | J. Phys. Chem. C 2014, 118, 4991−4997

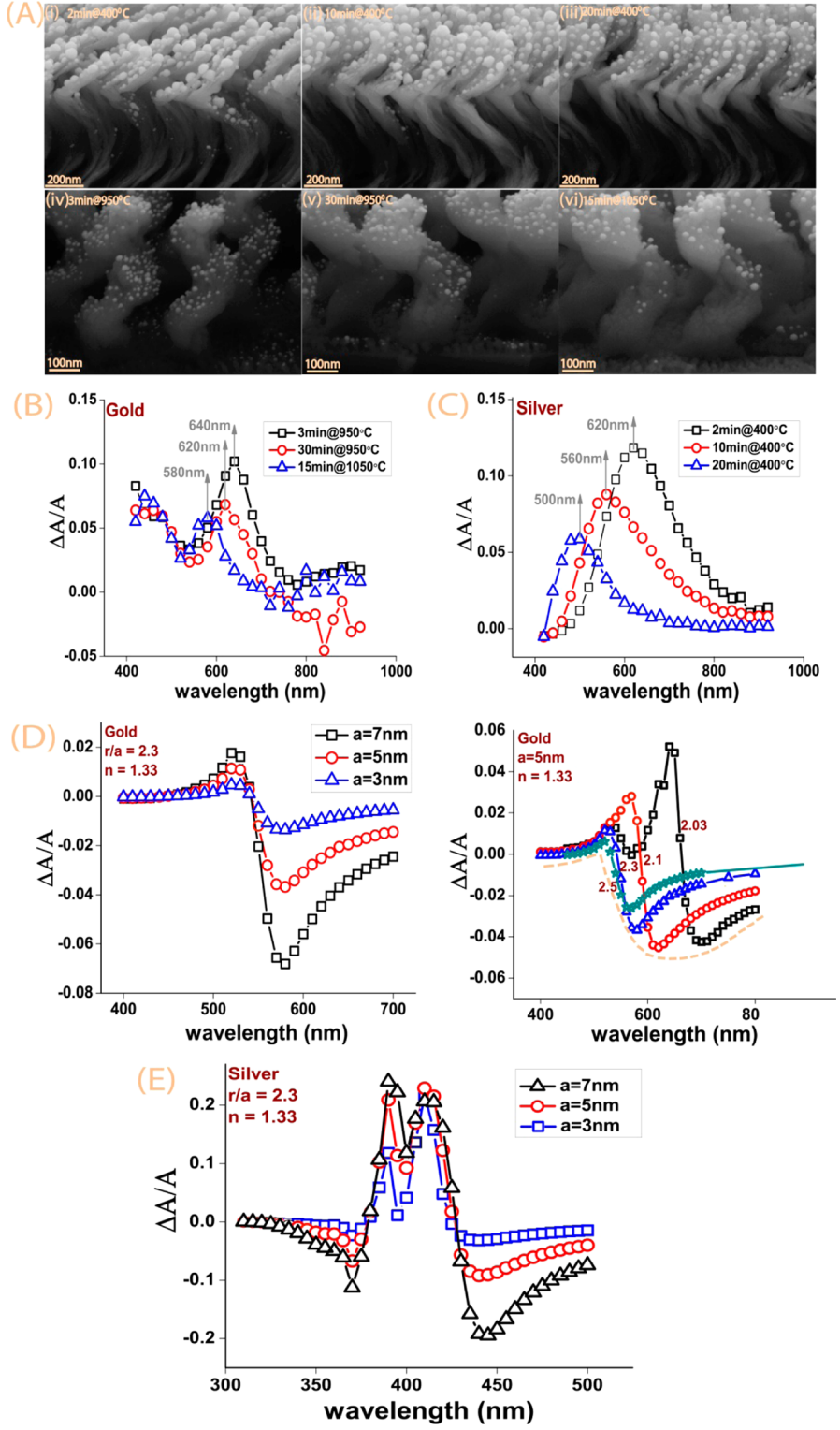

Figure 3. (A) SEM images of a chiroplasmonic metamaterial containing Ag (upper row) and Au NPs (lower row) decorating a helically nanostructured thin film, made of SiO_2. By controlling the duration of annealing of the film around 1000 °C, the separations between the NPs could be varied in the range r/a from 2.1 to 4, without significant variation in the particle sizes (<20%). (B) Experimentally measured asymmetry factor as a function of wavelength for Au NPs for different annealing times and temperatures. Corresponding r/a (and a) values were found to be 2.57 ± 0.5 (7.4 ± 1.6 nm), 3.1 ± 0.9 (8.4 ± 1.9 nm), and 3.61 ± 0.9 (9.5 ± 1.6 nm). (C) Same as panel B, except for Ag, where the r/a (and a) values were found to be 2.44 ± 0.42 (15.2 ± 2 nm), 2.7 ± 0.6 (14.6 ± 2.7 nm), and 3.07 ± 0.7 (15.1 ± 2.8 nm) for different annealing times. (D) (Left panel) Calculation of the effect of variation of size of the Au NPs embedded in water on the chiroptical spectra, for fixed r/a = 2.3, showing negligible effect on λ_p and $\Delta\lambda$. (Right panel) Calculation of the effect of variation of r/a for Au NPs of radius 5 nm embedded in water, showing significant red shift and spectral broadening. The dotted line shows a possible convolution of the spectra arising from a distribution of r/a, as would be expected in the experimental system. (E) Effect of variation of the size of Ag NPs embedded in water on $\Delta A/A$ for fixed r/a = 2.3, showing small dependence of the chiroptical spectra on size.

dx.doi.org/10.1021/jp4117535 | J. Phys. Chem. C 2014, 118, 4991−4997

water. The details of the calculations and the results have been shown in the Supporting Information.

We believe the highly enhanced values of $\Delta\lambda$ and λ_p of the measured spectra were due to the variability in size and spacing of the NPs in the experimental system. Of these, the role of size variation was found to affect only the strength of the interaction, that is, $\Delta A/A$, and not λ_p and $\Delta\lambda$, when r/a was assumed to be constant. This is shown in Figure 3D (left panel) and Figure 3E for three sizes of Au and Ag NPs, assuming r/a to be 2.3 for all spectra. On the contrary, assuming a fixed particle size but varying r/a resulted in large changes of the λ_p and $\Delta\lambda$, which is shown in the right panel of Figure 3D (for Au). A possible convolution of r/a ranging from 2.03 to 2.5 is shown schematically with a dotted line, resulting in a broad and highly red-shifted spectrum, which can correspond to a realistic experimental scenario, for example, in the results shown in Figure 3B. A similar effect of r/a variation can explain the differences between the numerical calculations (Figure 1C) and experimental results (Figure 3C) for Ag. These observations automatically suggest a possible design rule toward obtaining broadband chiroptical devices, a system where contributions from multiple r/a geometries could be combined to have large enhancement of the spectral width.

One important application arising from chiral metamaterials is the enhancement of chiroptical signals of biomolecules located in the vicinity of such structures. The origin of this enhancement lies in the structure of the electromagnetic fields, which is commonly quantified in terms of the parameter "optical chirality", defined as $C(\vec{r}) = -((\epsilon_0 w)/2)\ \mathrm{Im}[\vec{E}^*(r)\cdot\vec{B}(r)]$,[31,40] where $\vec{E}(r)$ and $\vec{B}(r)$ refer to the complex field amplitudes and w is the frequency of the EM wave. It can be shown that the circular differential rate of excitation of a chiral molecule present at a position $\vec{r}$ is proportional to $\Delta C = (C^+(\vec{r}) - C^-(\vec{r}))/|C^{CPL}(\vec{r})|$,[40] where $\pm$ refers to left and right circular polarization states of the incident wave, respectively, and $C^{CPL}\vec{r}$ refers to the optical chirality of the field in the absence of the nanostructure. As we show here, the differential optical chirality (ΔC) of the NP complex discussed in this paper can be very large at small r/a, in fact higher than what could be obtained with any nanoplasmonic system developed so far. This study is extremely relevant to the experimental system presented here, as the nanostructured films described here are inherently porous, which may allow the chiral molecules to easily diffuse in a region of high differential optical chirality. The results of the numerical calculations of ΔC for a particular geometry with r/a = 2.1 are shown in Figure 4A, corresponding to different planar slices perpendicular to the helical axis. It is interesting to note that the magnitude of the differential optical chirality is highest at the junction between the NPs (highly accessible in the present experimental system) and falls off to zero very rapidly away from it. The maximum possible magnitude of ΔC for a particular helical geometry, given by ΔC_{max}, depended strongly on r/a, as shown in Figure 4B. The highest ΔC_{max} obtained in our study was almost 3000 (for r/a = 2.03), which is higher than all other chiroplasmonic structures investigated so far, including solid Au helices[41] ($\Delta C_{max} \approx 7$), planar gammadions[23] ($\Delta C_{max} \approx 20$), plasmonic spit-ring resonators[42] ($\Delta C_{max} \approx 30$), and 3-D chiral plasmonic oligomers[43] ($\Delta C_{max} \approx 100$). We will test these theoretical predictions in the future to see if the nanostructured film presented here can indeed be used for improved enantiomeric sensing applications. Similar to previous studies on 2-D chiral gammadions,[23] we expect a modification

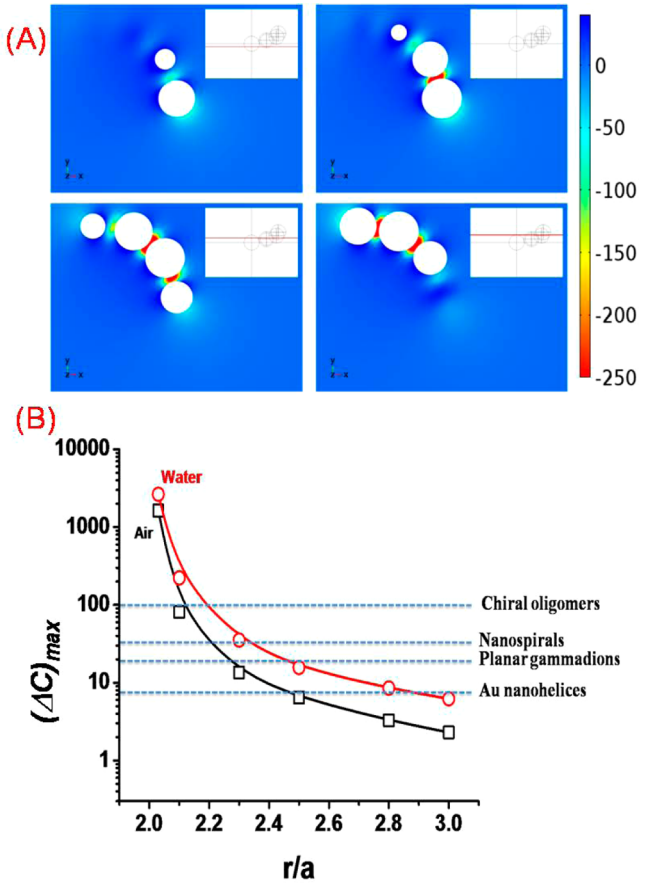

Figure 4. (A) Plot of ΔC, differential enhancement of optical chirality (see the main text for definition and details), for various planes perpendicular to the helix axis containing four Au NPs embedded in water. We assumed a = 5 nm and r/a = 2.1 in these numerical simulations. The positions of the slices are shown in the inset (red lines). (B) Plot of ΔC_{max}, maximum possible magnitude of ΔC, around the NP complex for different values of r/a. The NPs are assumed to be made of Au with radius 5 nm, and the surrounding medium was assumed to be either air or water. Also shown are comparisons of ΔC_{max} obtained with various other nanoplasmonic geometries.

of the chiroptical spectra of the substrates discussed in this manuscript upon adsorption of the chiral molecules.

CONCLUSIONS

In summary, we have investigated the chiroptical properties of noble-metal NPs arranged in a helical geometry, in particular, when the particles are in close separation. As the NPs are brought closer, the asymmetry factor rises in an almost exponential fashion, while the spectra become highly red-shifted with significant enhancement of the spectral width. We investigated these phenomena with a novel experimental system of dielectric helical templates decorated by spherical Au and Ag NPs and obtained a very large chiroptical signal covering a large portion of the visible range of the electromagnetic spectrum. The spectral width of the experimental system was further enhanced due to the variability of the size and spacing of the NPs, a principle that can be used to develop chiral metamaterials with broadband response in the visible. Furthermore, we investigated the suitability of this system as an enantiomeric detector, by calculating the "optical chirality" of the EM fields around the NP complex. The theoretical analysis predicts an enhancement of the molecular

dx.doi.org/10.1021/jp4117535 | J. Phys. Chem. C 2014, 118, 4991−4997

chiroptical signal far more than what could be obtained with presently available nanoplasmonic geometries, an effect that increases dramatically at small particle separations.

METHODS

Numerical Simulations: DDASCAT. In this study, discrete dipole approximations (DDAs)[33] were one of the methods used to simulate the chiroptical response of the helical nanostructures decorated with metallic NPs with very small gaps ($r < 3a$) between them. The target structure (metal NPs) was discretized into a lattice of polarizable dipole volumes, and this discretization was optimized with respect to the target size and the maximum allowed error for an effective convergence. The complex permittivity for gold was extracted from past measurements.[32] The polarizability of the dipoles is computed from the permittivity using the lattice-dispersion relations.[44] Here the helical structure of radius 18 nm and pitch 25 nm consisted of four gold NPs, each consisting of 2176 dipoles (16 dipoles across the diameter of the sphere). The modeled incident circularly polarized beam was propagating along the axis of the helix. The NPs on a single helix were considered for the near-field calculations as opposed to an entire lattice of helices used in the experiments discussed later, because the distance between the adjacent helices is relatively large compared with the distance between neighboring NPs of the same helix.

Numerical Simulations: FEM-Comsol. We used numerical simulation software Comsol Multiphysics 4.3a,[35] a finite element method-based solver to cross-check the results calculated with DDASCAT. In the present case, the model geometry consisted of four metal NPs (Au or Ag) arranged in a helical fashion. We used a spherical PML of thickness 200 nm and order one surrounding the model geometry. The PML was placed at half-wavelength away from the metal NPs so that it was not within the near-field region of the metal NPs.[34] The entire structure was divided into domains and subdomains, and each domain was meshed using free tetrahedral meshing of maximum size of six elements per wavelength outside the metallic spheres and a maximum element size of 13.5 nm (for Au) inside the spheres to obtain optimal convergence.[34] We assumed the incident beam to be circularly polarized, propagating parallel to the helix axis. The frequency-dependent complex dielectric function of the metal NPs was taken from ref 32. We adopt iterative solver to solve the wave equation, such as to calculate the absorption cross section. Sweep parameter was used to scan the wavelength range from 400 to 850 nm.

Fabrication. The samples were fabricated[37] based on a physical vapor deposition technique known as glancing angle deposition (GLAD).[45] First a dielectric helical template made up of SiO_2 (∼500 nm thickness) was fabricated using the conventional GLAD technique where a rotating (0.05 to 0.1 rpm) glass substrate was kept at an extreme angle of 84° to the incoming vapor source (0.1 to 0.2 nm/second). In the second step, the substrate angle was reduced to around 5°, and a small amount of metal (3 nm for Au and 6 nm for Ag) was evaporated on the glass substrate at the rate of ∼0.01 nm/second, resulting in the formation of randomly oriented isolated metal islands on the surface of the helices by self-shadowing effect. These metal-decorated helices were annealed at different temperatures (∼400 °C for Ag and ∼1000 °C for Au) for different timings in a metal-annealing furnace under Argon ambient, such as to improve particle sphericity as well as to control their spacing. The samples were allowed to cool to room temperature before the optical measurements were taken.

Optical Characterization. The films containing metal-decorated helices were optically characterized by measuring their chiroptical response, namely, CD, using photoelastic modulation technique coupled to standard phase-locked detection scheme. Light of a particular wavelength emitting from the monochromator (Horiba Yvon) was sent to a photoelastic modulator (Hinds Instruments), which modulates between left and right circularly polarized states at 42 kHz and transmitted normally through the substrate and then onto the photodetector (Thorlabs). The cable lengths and the load resistance across the photodiode were kept sufficiently low to ensure the temporal response of the detector to be faster than 150 kHz. The CD signal was measured though a lock-in amplifier (Signal Recovery 7270) through standard phase-locked detection techniques. The absorbance of the samples used in the estimate of the anisotropy factor was measured using an USB spectrometer (Ocean Optics).

ASSOCIATED CONTENT

Supporting Information

Details of the semianalytical calculations; effect of dielectric template; comparison between the simulation results of FEM and DDASCAT as mentioned in the text; and typical CD spectrum corresponding to Figure 1B. This material is available free of charge via the Internet at http://pubs.acs.org.

AUTHOR INFORMATION

Corresponding Author

*E-mail: ambarish@ece.iisc.ernet.in.

Author Contributions

⊥G.N. and H.J.S. contributed equally.

Notes

The authors declare no competing financial interest.

ACKNOWLEDGMENTS

We thank Santhanam Venugopal for his help with the optical measurement system and Department of Biotechnology (DBT) and Space Technology Cell (STC) for funding this work and gratefully acknowledge the usage of the facilities in Advanced Facility for Microscopy and Microanalysis (AFMM) and Micro and Nano Characterization Facility (MNCF, CeNSE) at IISc. This work is partially supported by the Ministry of Communication and Information Technology under a grant for the Centre of Excellence in Nanoelectronics, Phase II.

REFERENCES

(1) Maier, S. *Plasmonics: Fundamentals and Applications*; Springer: New York, 2007.

(2) Huang, X.; El-Sayed, I. H.; Qian, W.; El-Sayed, M. A. Cancer Cell Imaging and Photothermal Therapy in the Near-Infrared Region by Using Gold Nanorods. *J. Am. Chem. Soc.* **2006**, *128*, 2115−2120.

(3) Lee, K.-S.; El-Sayed, M. A. Gold and Silver Nanoparticles in Sensing and Imaging: Sensitivity of Plasmon Response to Size, Shape, and Metal Composition. *J. Phys. Chem. B* **2006**, *110*, 19220−19225.

(4) Citrin, D. Coherent Excitation Transport in Metal-Nanoparticle Chains. *Nano Lett.* **2004**, *4*, 1561−1565.

(5) Haynes, C. L.; McFarland, A. D.; Zhao, L.; Duyne, R. P. V.; Schatz, G. C.; Gunnarsson, L.; Prikulis, J.; Kasemo, B.; Käll, M. Nanoparticle Optics: The Importance of Radiative Dipole Coupling in Two-Dimensional Nanoparticle Arrays. *J. Phys. Chem. B* **2003**, *107*, 7337−7342.

(6) Maier, S. A.; Brongersma, M. L.; Kik, P. G.; Atwater, H. A. Observation of Near-Field Coupling in Metal Nanoparticle Chains Using Far-Field Polarization Spectroscopy. *Phys. Rev. B* **2002**, *65*, 193408.
(7) Zhao, L.; Kelly, K. L.; Schatz, G. C. The Extinction Spectra of Silver Nanoparticle Arrays: Influence of Array Structure on Plasmon Resonance Wavelength and Width. *J. Phys. Chem. B* **2003**, *107*, 7343−7350.
(8) Antosiewicz, T. J.; Apell, S. P.; Zäch, M.; Zorić, I.; Langhammer, C. Oscillatory Optical Response of an Amorphous Two-Dimensional Array of Gold Nanoparticles. *Phys. Rev. Lett.* **2012**, *109*, 247401.
(9) Hanarp, P.; Käll, M.; Sutherland, D. S. Optical Properties of Short Range Ordered arrays of Nanometer gold Disks Prepared by Colloidal Lithography. *J. Phys. Chem. B* **2003**, *107*, 5768−5772.
(10) Zoric, I.; Zach, M.; Kasemo, B.; Langhammer, C. Gold, Platinum, and Aluminum Nanodisk Plasmons: Material Independence, Subradiance, and Damping Mechanisms. *ACS Nano* **2011**, *5*, 2535−2546.
(11) Mark, A. G.; Gibbs, J. G.; Lee, T. C.; Fischer, P. Hybrid Nanocolloids with Programmed Three-Dimensional Shape and Material Composition. *Nat. Mater.* **2013**, *12*, 802−807.
(12) Singh, H. J.; Ghosh, A. Porous Three Dimensional Arrays of Plasmonic Nanoparticles. *J. Phys. Chem. C* **2012**, *116*, 19467−19471.
(13) Guerrero-Martínez, A.; Alonso-Gómez, J. L.; Auguié, B.; Cid, M. M.; Liz-Marzán, L. M. From Individual to Collective Chirality in Metal Nanoparticles. *Nano Today* **2011**, *6*, 381−400.
(14) Guerrero-Martínez, A.; Auguié, B.; Alonso-Gómez, J. L.; Džolić, Z.; Gómez-Graña, S.; Žinić, M.; Cid, M. M.; Liz-Marzán, L. M. Intense Optical Activity from Three-Dimensional Chiral Ordering of Plasmonic Nanoantennas. *Angew. Chem.* **2011**, *50*, 5499−5503.
(15) Kuzyk, A.; Schreiber, R.; Fan, Z.; Pardatscher, G.; Roller, E.-M.; Högele, A.; Simmel, F. C.; Govorov, A. O.; Liedl, T. DNA-Based Self-Assembly of Chiral Plasmonic Nanostructures with Tailored Optical Response. *Nature* **2012**, *483*, 311−314.
(16) Rosi, N. L.; Song, C.; Blaber, M. G.; Zhao, G.; Zhang, P.; Fry, H. C.; Schatz, G. C. Tailorable Plasmonic Circular Dichroism Properties of Helical Nanoparticle Superstructures. *Nano Lett.* **2013**, *13* (7), 3256−3261.
(17) Liu, N.; Guo, H.; Fu, L.; Kaiser, S.; Schweizer, H.; Giessen, H. Three-dimensional Photonic Metamaterials at optical frequencies. *Nat. Mater.* **2007**, *7*, 31−37.
(18) Soukoulis, C. M.; Wegener, M. Past Achievements and Future challenges in the Development of Three-Dimensional Photonic Metamaterials. *Nat. Photonics* **2011**, *5*, 523−530.
(19) Pendry, J. B. A Chiral Route to Negative Refraction. *Science* **2004**, *306*, 1353−1355.
(20) Zhang, S.; Park, Y.-S.; Li, J.; Lu, X.; Zhang, W.; Zhang, X. Negative Refractive Index in Chiral Metamaterials. *Phys. Rev. Lett.* **2009**, *102*, 023901.
(21) Gansel, J. K.; Thiel, M.; Rill, M. S.; Decker, M.; Bade, K.; Saile, V.; Freymann, G.von.; Linden, S.; Wegener, M. Gold Helix Photonic Metamaterial as Broadband Circular Polarizer. *Science* **2009**, *325*, 1513−1515.
(22) Zhao, Y.; Belkin, M.; Alù, A. Twisted Optical Metamaterials for Planarized Ultrathin Broadband Circular Polarizers. *Nat. Commun.* **2012**, *3*, 870.
(23) Hendry, E.; Carpy, T.; Johnston, J.; Popland, M.; Mikhaylovskiy, R. V.; Lapthorn, A. J.; Kelly, S. M.; Barron, L. D.; Gadegaard, N.; Kadodwala, M. Ultrasensitive Detection and Characterization of Biomolecules Using Superchiral Fields. *Nat. Nanotechnol.* **2010**, *5*, 783−787.
(24) Fan, Z.; Govorov, A. O. Plasmonic Circular Dichroism of Chiral Metal Nanoparticle Assemblies. *Nano Lett.* **2010**, *10*, 2580−2587.
(25) Fan, Z.; Govorov, A. O. Helical Metal Nanoparticle Assemblies with Defects: Plasmonic Chirality and Circular Dichroism. *J. Phys. Chem. C* **2011**, *115*, 13254−13261.
(26) Park, S. Y.; Stroud, D. Surface-Plasmon Dispersion Relations in Chains of Metallic Nanoparticles: An Exact Quasistatic Calculation. *Phys. Rev. B* **2004**, *69*, 125418.
(27) Weber, W. H.; Ford, G. W. Propagation of Optical Excitations by Dipolar Interactions in Metal Nanoparticle Chains. *Phys. Rev. B* **2004**, *70*, 125429.
(28) Nordlander, P.; Oubre, C.; Prodan, E.; Li, K.; Stockman, M. I. Plasmon Hybridization in Nanoparticle Dimers. *Nano Lett.* **2004**, *4*, 899−903.
(29) Gunnarsson, L.; Rindzevicius, T.; Prikulis, J.; Kasemo, B.; Käll, M.; Zou, S.; Schatz, G. C. Confined Plasmons in Nanofabricated Single Silver Particle Pairs: Experimental Observations of Strong Interparticle Interactions. *J. Phys. Chem. B* **2005**, *109*, 1079−1087.
(30) Jain, P. K.; Huang, W.; El-Sayed, M. A. On the Universal Scaling Behavior of the Distance Decay of Plasmon Coupling in Metal Nanoparticle Pairs: A Plasmon Ruler Equation. *Nano Lett.* **2007**, *7*, 2080−2088.
(31) Schäferling, M.; Dregely, D.; Hentschel, M.; Giessen, H. Tailoring Enhanced Optical Chirality: Design Principles for Chiral Plasmonic Nanostructures. *Phys. Rev. X* **2012**, *2*, 031010.
(32) Johnson, P. B.; Christy, R. W. Optical Constants of the Noble Metals. *Phys. Rev. B* **1972**, *6*, 4370.
(33) Draine, B. T.; Flatau, P. J. Discrete-Dipole Approximation for Periodic Targets: Theory and Tests. *J. Opt. Soc. Am. A* **2008**, *25*, 2693−2703.
(34) COMSOL Multiphysics RF Module 4.3a User's Guide.
(35) *Comsol Multiphysics Simulation Software*, version 4.3a, 2012. www.comsol.com.
(36) Markel, V. A. Coupled-Dipole Approach to Scattering of Light From a One-Dimensional Periodic Dipole Structure. *J. Mod. Opt.* **1993**, *40*, 2281−2291.
(37) Singh, J. H.; Nair, G.; Ghosh, A.; Ghosh, A. Wafer Scale Fabrication of Porous Three Dimensional Plasmonic Metamaterials for the Visible: Chiral and Beyond. *Nanoscale* **2013**, *5*, 7224−7228.
(38) Jensen, T. R.; Malinsky, M. D.; Haynes, C. L.; Van Duyne, R. P. Nanosphere Lithography: Tunable Localized Surface Plasmon Resonance Spectra of Silver Nanoparticles. *J. Phys. Chem. B* **2000**, *104*, 10549−10556.
(39) Tan, B. J. Y.; Sow, C. H.; Koh, T. S.; Chin, K. C.; Wee, A. T. S.; Ong, C. K. Fabrication of Size-Tunable Gold Nanoparticles Array with Nanosphere Lithography, Reactive ion Etching, and Thermal Annealing. *J. Phys. Chem. B* **2005**, *109*, 11100−11109.
(40) Tang, Y.; Cohen, A. E. Optical Chirality and its Interaction with Matter. *Phys. Rev. Lett.* **2010**, *104*, 163901.
(41) Gansel, J. K.; Wegener, M.; Burger, S.; Linden, S. Gold Helix Photonic Metamaterials: A Numerical Parameter Study. *Opt. Express* **2010**, *18*, 1059−1069.
(42) Liu, N.; Liu, H.; Zhu, S.; Giessen, H. Stereometamaterials. *Nat. Photonics* **2009**, *3*, 157−162.
(43) Hentschel, M.; Schäferling, M.; Weiss, T.; Liu, N.; Giessen, H. Three-Dimensional Chiral Plasmonic Oligomers. *Nano Lett.* **2012**, *12*, 2542−2547.
(44) DeVoe, H. Optical Properties of Molecular Aggregates. I. Classical Model of Electronic Absorption and Refraction. *J. Chem. Phys.* **1964**, *41*, 393.
(45) Robbie, K.; Brett, M. Sculptured Thin Films and Glancing Angle Deposition: Growth Mechanics and Applications. *J. Vac. Sci. Technol., A* **1997**, *15*, 1460−1465.